

In vitro fluid dynamic measurements as a support of the cardiovascular Patient Specific Diagnosis

Giorgio Querzoli^{1*}, Vittorio Satta¹, Gildo Matta², Simone Ferrari¹, Maria Grazia Badas¹, Matteo Pibiri¹, Elena Sica¹, Grazia Bitti²

¹Università di Cagliari, DICAAR, Italy

² G. Brotzu Hospital, Department of Radiology, Cagliari, Italy

*querzoli@unica.it

Abstract

Under the project “Patient Specific Diagnosis (PSD) for Cardiovascular Diseases”, funded by the Regional Government of Sardinia (Italy), an innovative collaboration has been established between engineers (group of Hydraulics at the DICAAR – University of Cagliari, Italy) and physicians (group of the Department of Radiology of the Brotzu Hospital in Cagliari, Italy), in order to set-up and test a patient specific modeling procedure, based on the in vitro study of the cardiovascular fluid mechanics to the support of the physical interpretation of the diagnostic imaging data. The method consists of identifying the geometry of the vessels from diagnostic images, building up a mock vessel made of silicon rubber, inserting the model in a pulse duplicator able to reproduce the pulsatile blood flow, and investigating the flow by means of velocimetry techniques based on the image analysis. The results can be shared with the physicians in order to potentially support the interpretation of the information obtained by means of the diagnostic imaging.

1 Introduction

The continuous development of the cardiovascular diagnostic imaging techniques yields the detailed volumetric information needed to perform accurate fluid-dynamic simulations. On the other hand, the growing availability of cardiovascular flow datasets that can be gathered in vivo generate an increasing demand for physically based interpretation. That aspect is particularly important for the left ventricle and thoracic aorta, a district where the flow is of prominent importance. As a matter of fact, nowadays, routine diagnostic tests, such as computed tomography angiography or magnetic resonance, yield complete information about the geometry of the aorta and left ventricle. Additionally, Magnetic Resonance can give space- and time-resolved information about the blood flow in the thoracic aorta (Kvitting et al. 2004; Mirabella et al. 2014). Such a huge amount of data is potentially very useful to the early diagnosis of cardiovascular diseases (Teixido-Tura et al. 2014; Cordero et al. 2015). However, in order to educe useful diagnostic indications, a physically based interpretation is required. In the last decades, the fluid dynamics of patient specific geometries has been investigated mostly by means of computational fluid mechanics (Saber et al. 2003; Vedula et al. 2014; Bosi et al. 2015; Bonfanti et al. 2017) due to the complex geometry of the vessels. However, the recent

improvement of the additive manufacturing (the so-called 3D printing) allows the realization of accurate patient specific models derived from volumetric diagnostic imaging (Giannopoulos et al. 2016; Vukicevic et al. 2017). This technology was experimented as a support to the planning of surgical operations (Sodian et al. 2008), implantation of Left Ventricular Assist Devices (Farooqi et al. 2016) or prosthetic transcatheter valves (Wang et al. 2016) and can be used to realize transparent models that make possible the in vitro investigation of the patient specific cardiovascular fluid mechanics. In vitro modeling can be a powerful tool, complementary to the computational fluid dynamics, for the physical interpretation of the diagnostic imaging as far it allows running the experiments in controlled and repeatable conditions, which is not possible with the in vivo measurements. Additionally, in vitro testing allows the systematic modification of geometrical and flow characteristics in order to explore the sensitivity of the phenomenon to some parameters (Querzoli et al. 2014).

Hereafter, we present a methodology to investigate in vitro the fluid dynamics in patient specific geometries obtained from computed tomography angiography with contrast. The work was carried on within the project “Patient Specific Diagnosis (PSD) for Cardiovascular Diseases”, funded by the Regional Government of Sardinia (Italy): an innovative collaboration has been established between engineers (group of Hydraulics at the DICAAR – University of Cagliari, Italy) and physicians (group of the Department of Radiology of the Brotzu Hospital in Cagliari, Italy). The main goal of the project is to set-up and test a modeling procedure which allows the in vitro study of the cardiovascular fluid mechanics useful to the support of the physical interpretation of the diagnostic imaging data. The methodology allows a relatively fast and not expensive realization of transparent models, so that it is compatible with the continuous interaction and the trial-and-error process which is necessary for the clinical application of the methodology. The results we present focus on ascending aortas with different degrees of dilation, with the aim of elucidating the consequences on the flow pattern.

2 Materials and methods

The PSD procedure relies on the following steps:

- anonymised contrast-enhanced computed tomography (CT) images of the ascending aorta of a patient of interest are sent from the radiologists to the engineers;
- the contrast-enhanced CTs are segmented and a 3D-printed mold of the aorta is realized;
- silicon rubber is cast on the mold, in order to create a transparent and flexible model of the aorta (Querzoli et al. 2016);
- the model of the aorta is mounted in a laboratory mock-loop able to reproduce the physiological pulsatile flow;
- time-resolved evolution of the velocity fields is obtained by means of an image velocimetry technique (Besalduch et al. 2013);
- the flow fields are analyzed and the statistics are evaluated.

We performed the experiments in the mock-loop sketched in Figure 1. The pulsatile flow is generated by the alternative motion of a piston, driven by a linear motor, which changes the volume of the ventricular chamber (parallelepipedal, made of 20mm thick Plexiglas) that is connected to the hydraulic circuit through two check valves mimicking the aortic and mitral valves of the heart. The mitral valve was a hydraulic one-way membrane valve, whereas the aortic valve was made in house in order to reproduce the native aortic valve (Figure 2, right panel) as close as possible. The model

aorta was mounted inside the aortic chamber, parallelepipedal, with 10mm thick Plexiglas walls, and filled with water in order to allow the optical access and compensate the internal aortic pressure during the heart cycle (Figure 2, left panel). Downstream of the aortic chamber, two tunable valves and a vessel partially filled with air reproduced the impedance of the systemic circulation.

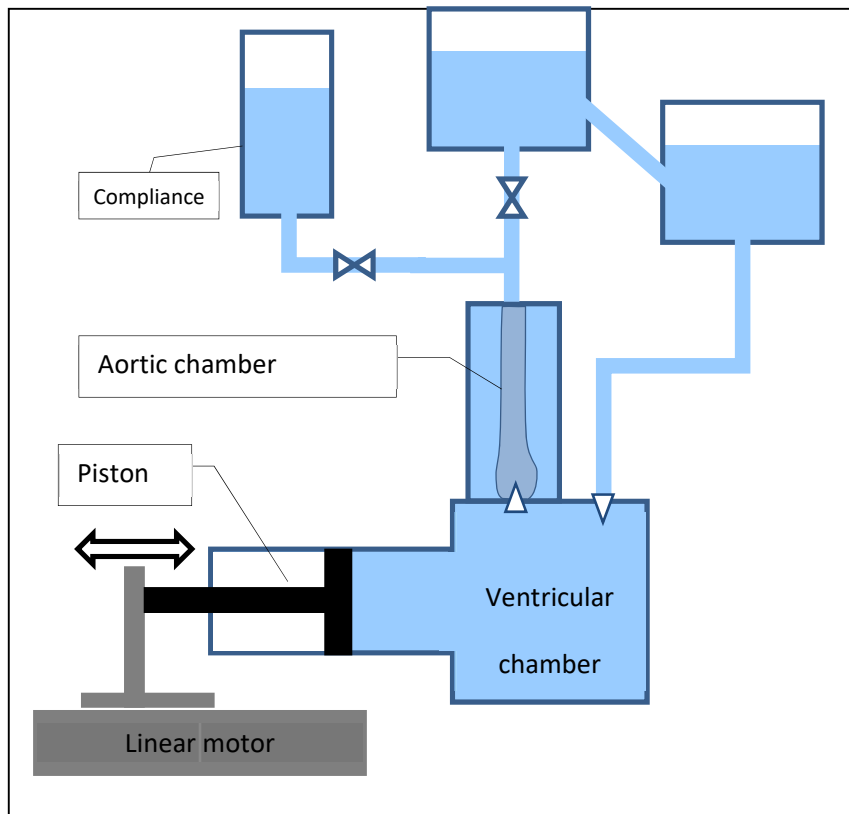


Figure 1: Sketch of the pulse duplicator used during the experiments

The geometry given by the CT was processed in order to adapt the model to the aortic chamber mountings. To this aim we considered a series of equispaced sections, normal to the main aortic axis and then we reported these sections on a rectilinear axis, thus obtaining the shape of the models displayed in Figure 3. As a consequence, the measurements can be considered representative only in the initial portion of the aortic artery where the vessel is substantially rectilinear, namely within the aortic root and the proximal ascending aorta.

The working fluid was seeded with pollen particles, 20 μm in diameter, and a plane of symmetry parallel to the vessel axis was illuminated by an infrared diode laser. A high-speed camera recorded 1111 frames per second with a resolution of 550 x 2240 pixels. Images were analyzed by means of the two-frames tracking algorithm described by Garau et al. (2018). Firstly the particles are recognized as Harris features (Harris and Stephens 1988) on the first frame; secondly, interrogation windows centered on the features in the first frame are compared to shifted windows on the second frame by means of the Lorentzian dissimilarity measure (Falchi et al. 2006), which is robust to the appearance and/or disappearance of particles and to high velocity gradients. The shift minimizing the dissimilarity, divided by the time interval between frames is assumed to be the fluid velocity.

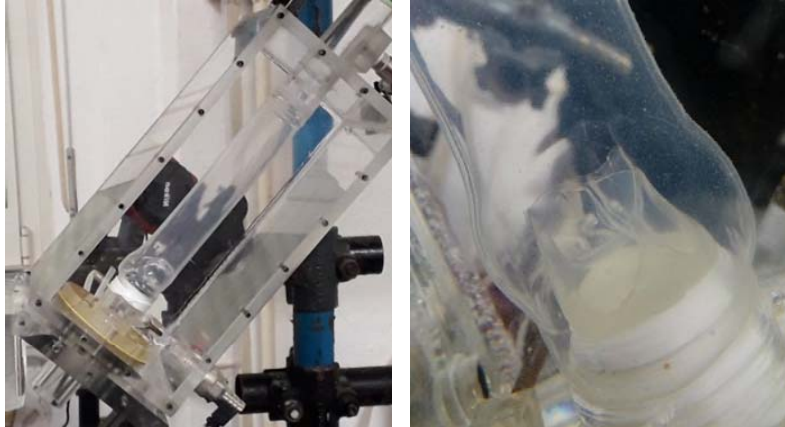


Figure 2: Left panel: aortic chamber; right panel: silicon aortic valve made in house



Figure 3: Aorta models used during the tests. Top panel: aneurismatic aorta 48mm; bottom panel: aneurismatic aorta 64mm

The sparse velocity samples at each instant are validated in order to discard the outliers and then used to compute the phase averages on a regular grid (41x131 nodes).

We considered two aortas with increasing degree of dilation: the first was aneurismatic with a maximum diameter of 48mm, i.e. close to the indication to the surgical intervention, and the second with a severe aneurism of the aortic root and a maximum diameter of 64mm (Figure 3). We simulated typical flowrate conditions, i.e. stroke volume $SV = 64\text{ml}$, and beat rate = 70 beats per minute (period $T = 0.86\text{s}$), thus resulting in a cardiac output $CO = 4.48$ liters per minute. Since we used distilled water as working fluid, which has a kinematic viscosity about 1/3 compared to the viscosity of the blood, in order to fulfill the dynamic similarity, i.e. the constancy of the Reynolds ($Re = UD/\nu$) and Womersley ($Wo = \sqrt{\left(\frac{D^2}{\nu T}\right)}$) we reduced the beat rate proportionally (for a detailed discussion see Cenedese et al. (2005) where U is the peak systolic velocity though the aortic valve, D is the diameter of the aortic valve, ν is the kinematic viscosity, and T is the period of the cardiac cycle. Therefore, during the experiments the stroke volume was $SV = 64\text{ml}$ and the period was $T = 2.57\text{s}$. The flow rate as a function of time is shown in Figure 4. We acquired 90 cycles for each aortic configuration and hereafter we present the phase averaged velocity fields.

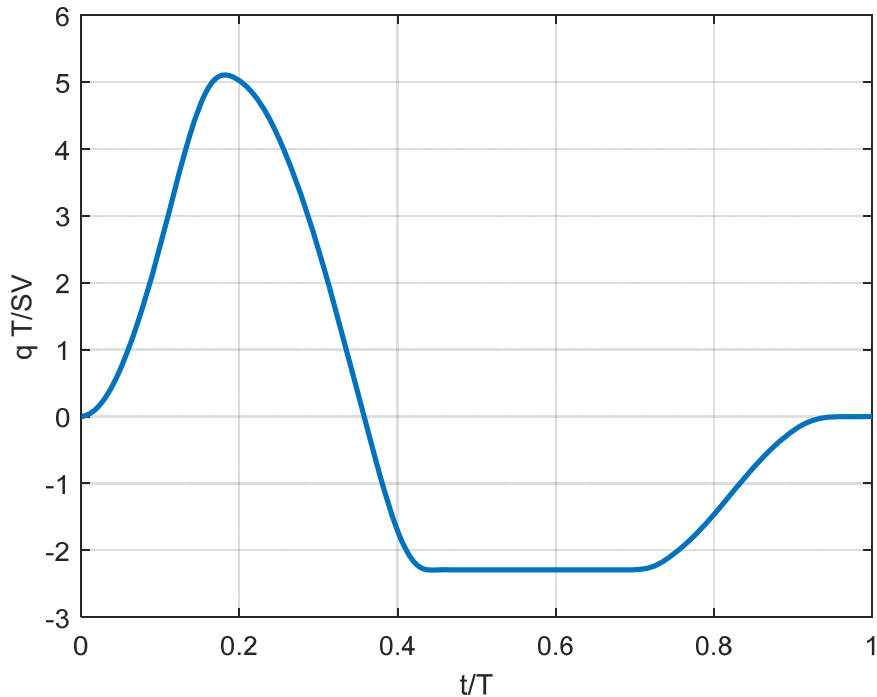


Figure 4: Non-dimensional transvalvular flow rate as a function of time

3 Results

Figures 5-8 show the phase averaged velocity fields at the most significant time instants of the cardiac cycle. At $t/T = 0.05$, i.e. at the beginning of the systole (Figure 5), the transvalvular jet is just at the beginning of its development. Two vortices are apparent in the aortic root, irrespective of the degree of dilation, however in the case of the 64mm dilation, the large volume of the sinus of Valsava (in the bottom of the figure) permits the growth of a larger vortex. The difference in the evolution of the vortices continue during the accelerating phase of the systole and, at the systolic peak ($t/T = 0.2$, Figure 6), and only one vortex is observed in the 48mm aorta, whereas in the 64mm aorta two large vortex are still developing. The different vortical structure has the consequence of redirecting the transvalvular jet. As a matter of fact, in the 64 mm aorta the symmetrical vortices allow the development of a centered jet, whereas in the 48mm, the dominating upper vortex tends to bend the jet in the opposite direction, i.e. towards the lower vascular wall in the figure.

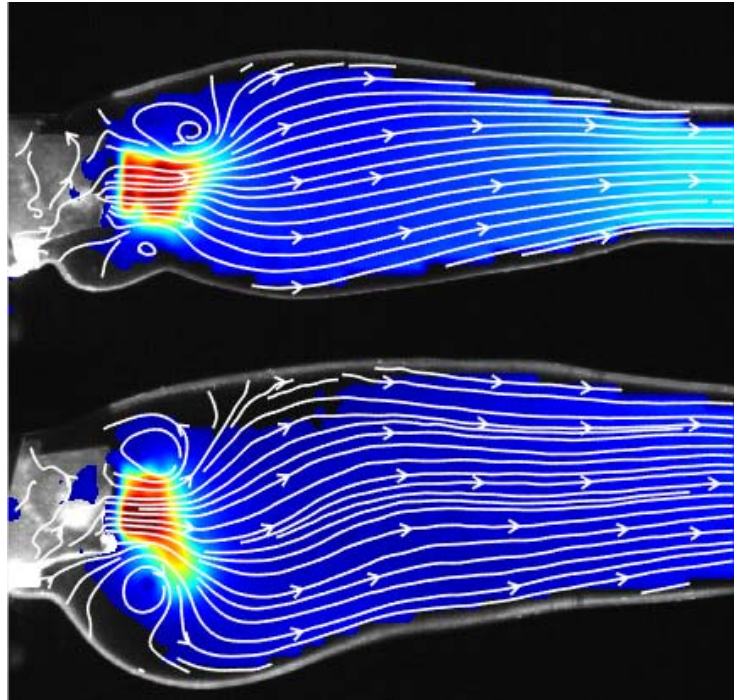


Figure 5: Mean velocity field at the beginning of the systole, $t/T = 0.05$. Top panel: 48mm dilation aorta; bottom panel: 64mm dilation aorta. Color indicates the velocity magnitude

During the decelerated ejection ($t/T = 0.30$, Figure 7) the transvalvular jet loses its strength, and the large volume of the ascending aorta permits the development of large jets, irrespective of the degree of dilation. At this stage of the cycle the upper vortex is dominant and the jet is bent downwards. However, in the case of the 64mm dilation, the presence of the second vortex, proximal to the sinus of Valsalva, redirects the transvalvular jet so that it impinges the vascular wall well downstream of the aortic root. Conversely, in the case of 48mm dilation, that vortex is not present and the jet reaches the wall just at the sinotubular junction.

At the end of the systole ($t/T = 0.40$, Figure 8), the flow in the ascending aorta is reorganized in a large, single vortex both in the 48mm and in the 64mm aorta. Interestingly, in this case, only the 48mm aorta exhibits a vortex in the proximity of the sinus of Valsalva. As expected, at this stage the velocity magnitudes are low. In both cases the streamlines give evidence of a backflow region in the distal aorta (right side of the figures). However, especially in the case of the 64mm dilation, the distal backflow region is basically separated from the recirculating region proximal to the aortic root.

4 Conclusions

We presented a methodology to test, in vitro, patient specific models of the ascending aorta. In order to demonstrate the procedure, we compared two aortic geometries of different degree of dilation. The results provide the evidence that the different shape of the vessel promotes a different development of the vortices originating during the propagation of the transvalvular jet.

The presence of the vortices in the aortic root tends to redirect the transvalvular jet during its propagation thus changing the region of impingement on the vascular wall. This modification, in turn, changes the maximum wall shear-stress distribution, with potential consequences on the thrombogenesis and on the organization of the endothelial cells. Significant changes are observed also in the recirculating flow at the end of the systole, even if, in that case, the structure of the flow is quite similar.

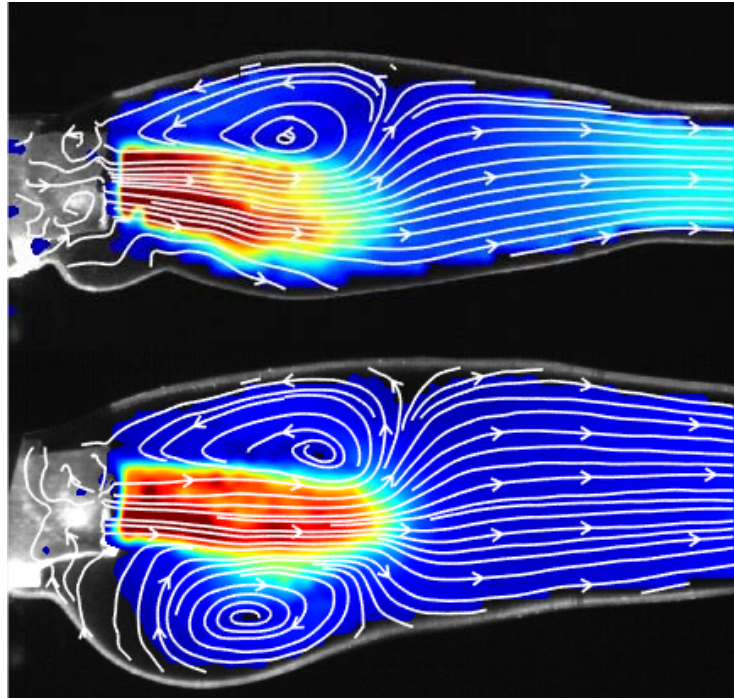


Figure 6: Mean velocity field at the systolic peak, $t/T = 0.20$. Top panel: 48mm dilation aorta; bottom panel: 64mm dilation aorta. Color indicates the velocity magnitude

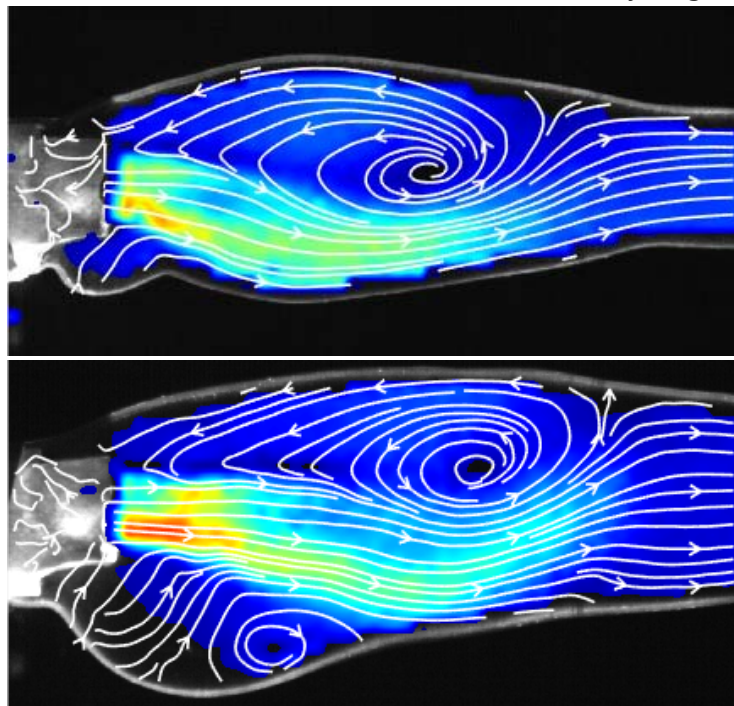


Figure 7: Mean velocity field at the decelerated ejection, $t/T = 0.30$. Top panel: 48mm dilation aorta; bottom panel: 64mm dilation aorta. Color indicates the velocity magnitude.

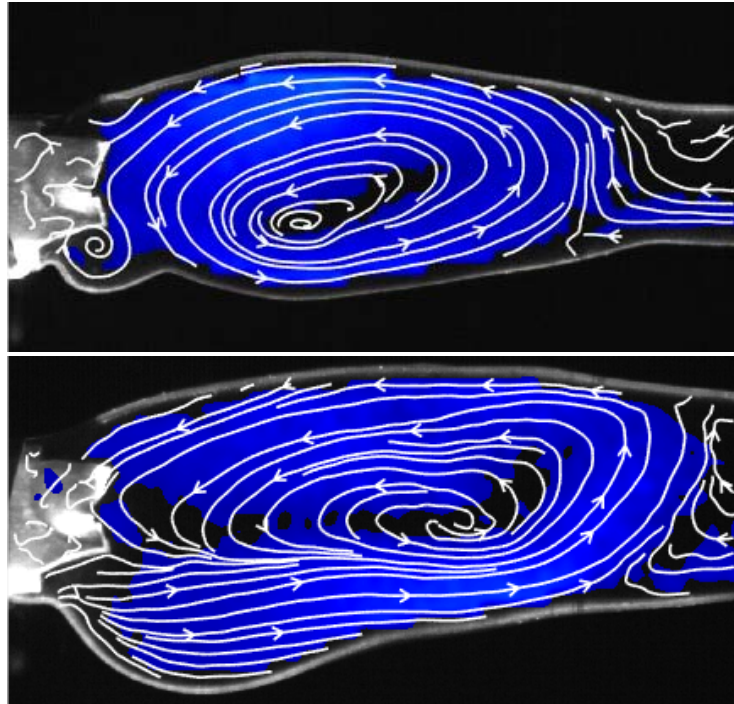


Figure 8: Mean velocity field at the decelerated ejection, $t/T = 0.30$. Top panel: 48mm dilation aorta; bottom panel: 64mm dilation aorta. Color indicates the velocity magnitude.

Acknowledgements

The authors are grateful to Antonio Mascia for his valuable contribution in building the experimental set-up. This work is carried on within the project "PSD for Cardiovascular Diseases (Patient Specific Diagnostics for Cardiovascular Diseases)", funded by the Sardinian Regional Government through the Public Procedure "Promozione di nuovi mercati per l'innovazione nella PA" under the POR FESR Sardegna 2014/2020

References

- Besalduch LA, Badas MG, Ferrari S, Querzoli G (2013) Experimental Studies for the characterization of the mixing processes in negative buoyant jets. EPJ Web of Conferences 45:01012. doi: 10.1051/epjconf/20134501012
- Bonfanti M, Balabani S, Greenwood JP, et al (2017) Computational tools for clinical support: a multi-scale compliant model for haemodynamic simulations in an aortic dissection based on multi-modal imaging data. Journal of The Royal Society Interface 14:20170632. doi: 10.1098/rsif.2017.0632
- Bosi GM, Capelli C, Khambadkone S, et al (2015) Patient-specific finite element models to support clinical decisions: A lesson learnt from a case study of percutaneous pulmonary valve implantation. Cathet Cardiovasc Intervent 86:1120–1130. doi: 10.1002/ccd.25944

Cenedese A, Prete ZD, Miozzi M, Querzoli G (2005) A laboratory investigation of the flow in the left ventricle of a human heart with prosthetic, tilting-disk valves. *Exp Fluids* 39:322–335. doi: 10.1007/s00348-005-1006-4

Cordero CD, Rossini L, Martinez-Legazpi P, et al (2015) PREDICTION OF INTRAVENTRICULAR THROMBOSIS BY QUANTITATIVE IMAGING OF STASIS: A PILOT COLOR-DOPPLER STUDY IN PATIENTS WITH ACUTE MYOCARDIAL INFARCTION. *J Am Coll Cardiol* 65:. doi: 10.1016/S0735-1097(15)61310-9

Falchi M, Querzoli G, Romano GP (2006) Robust evaluation of the dissimilarity between interrogation windows in image velocimetry. *Exp Fluids* 41:279–293. doi: 10.1007/s00348-006-0148-3

Farooqi KM, Saeed O, Zaidi A, et al (2016) 3D Printing to Guide Ventricular Assist Device Placement in Adults With Congenital Heart Disease and Heart Failure. *JACC: Heart Failure* 4:301–311. doi: 10.1016/j.jchf.2016.01.012

Garau M, Badas MG, Ferrari S, et al (2018) Turbulence and Air Exchange in a Two-Dimensional Urban Street Canyon Between Gable Roof Buildings. *Boundary-Layer Meteorol* 167:123–143. doi: 10.1007/s10546-017-0324-4

Giannopoulos AA, Mitsouras D, Yoo S-J, et al (2016) Applications of 3D printing in cardiovascular diseases. *Nat Rev Cardiol* 13:701–718. doi: 10.1038/nrcardio.2016.170

Harris C, Stephens M (1988) A combined corner and edge detector. In: *Alvey vision conference*. Citeseer, pp 10–5244

Kvitting J-PE, Ebberts T, Wigström L, et al (2004) Flow patterns in the aortic root and the aorta studied with time-resolved, 3-dimensional, phase-contrast magnetic resonance imaging: implications for aortic valve-sparing surgery. *The Journal of Thoracic and Cardiovascular Surgery* 127:1602–1607. doi: 10.1016/j.jtcvs.2003.10.042

Mirabella L, Barker AJ, Saikrishnan N, et al (2014) MRI-based Protocol to Characterize the Relationship Between Bicuspid Aortic Valve Morphology and Hemodynamics. *Ann Biomed Eng* 1–13. doi: 10.1007/s10439-014-1214-2

Querzoli G, Fortini S, Espa S, et al (2014) Fluid dynamics of aortic root dilation in Marfan syndrome. *Journal of Biomechanics* 47:3120–3128. doi: 10.1016/j.jbiomech.2014.06.025

Querzoli G, Fortini S, Espa S, Melchionna S (2016) A laboratory model of the aortic root flow including the coronary arteries. *Exp Fluids* 57:134. doi: 10.1007/s00348-016-2221-x

Saber NR, Wood NB, Gosman AD, et al (2003) Progress Towards Patient-Specific Computational Flow Modeling of the Left Heart via Combination of Magnetic Resonance Imaging with Computational Fluid Dynamics. *Annals of Biomedical Engineering* 31:42–52. doi: 10.1114/1.1533073

Sodian R, Weber S, Markert M, et al (2008) Pediatric cardiac transplantation: Three-dimensional printing of anatomic models for surgical planning of heart transplantation in patients with univentricular heart. *The Journal of Thoracic and Cardiovascular Surgery* 136:1098–1099. doi: 10.1016/j.jtcvs.2008.03.055

13th International Symposium on Particle Image Velocimetry – ISPIV 2019
Munich, Germany, July 22-24, 2019

Teixido-Tura G, Redheuil A, Rodríguez-Palomares J, et al (2014) Aortic biomechanics by magnetic resonance: Early markers of aortic disease in Marfan syndrome regardless of aortic dilatation? *International Journal of Cardiology* 171:56–61. doi: 10.1016/j.ijcard.2013.11.044

Vedula V, Fortini S, Seo J-H, et al (2014) Computational modeling and validation of intraventricular flow in a simple model of the left ventricle. *Theor Comput Fluid Dyn* 28:589–604. doi: 10.1007/s00162-014-0335-4

Vukicevic M, Mosadegh B, Min JK, Little SH (2017) Cardiac 3D Printing and its Future Directions. *JACC: Cardiovascular Imaging* 10:171–184. doi: 10.1016/j.jcmg.2016.12.001

Wang DD, Eng M, Greenbaum A, et al (2016) Predicting LVOT Obstruction After TMVR. *JACC: Cardiovascular Imaging* 9:1349–1352. doi: 10.1016/j.jcmg.2016.01.017